Adaptive Mesh Multi-Scale Modelling of Tidal Hydraulics and Material Transport,

S. Nash and M. Hartnett

Cite as:
Nash S and Hartnett M (2011) Adaptive Mesh Multi-Scale Modelling of Tidal Hydraulics and Material Transport. In: Topping BHV, Costa-Neves LF and Barros RC (eds.), *Proceedings of the Thirteenth International Conference on Civil, Structural and Environmental Engineering Computing*, Civil-Comp Press, Stirlingshire, UK, paper 107. doi:10.4203/ccp.96.107

Abstract

Multi-scale modelling for structured meshes is achieved by nesting high resolution grids within lower resolution grids. By specifying high resolutions in areas of interest only, computational cost can be reduced. Adaptive meshing can further optimise computational cost by allowing nested grids to change size and position in order to track a feature of interest such as a pollutant. This paper presents details of an adaptive mesh, multi-scale model for tidal hydraulics and mass transport in coastal waters. The model was used to simulate coliform discharges from a wastewater treatment plant in Galway Bay, Ireland. Results proved that the model is capable of predicting mass transport to a high degree of accuracy and that adaptive meshing provides an efficient alternative to the classical static grid nesting approach.

Keywords: adaptive mesh, multi-scale model, solute transport, coliforms

1 Introduction

In ocean and coastal modelling, high resolution is often required in a particular area of interest. In most cases, it is not the area itself that is of interest to the modeller but rather a process within the area such as a propagating wavefront or a discharge from a wastewater treatment plant. Nesting is an effective and established method of achieving high resolution in particular areas of a model domain without incurring the cost of high resolution across the whole domain. Most nested models to date employ static grids that are fixed in time and space [1, 2, 3]. For applications where the position and extents of the feature of interest do not change over time, classical static grid nesting techniques suffice. However, where the opposite is true, additional computational savings may be achieved by the use of moving grids whose positions and extents can change to match those of the feature of interest.

Moving grid nesting techniques, known as adaptive mesh techniques, have been in use in meteorological modelling for the last few decades [4, 5]. They are typically used in hurricane/cyclone/typhoon models where nesting is required to accurately resolve the storm core. Since these weather systems regularly travel thousands of kilometres it is not computationally efficient to specify a high resolution grid over the complete storm-path. Adaptive mesh multiple nested schemes are used instead; the adaptive mesh consists of multiple nests embedded in a telescopic fashion. The Geophysical Fluid Dynamics Laboratory (GFDL) hurricane model used by the National Oceanic and Atmospheric Administration (NOAA) in the United States uses such a scheme [6]. Adaptive mesh techniques were not introduced in the area of oceanographic modelling until the late nineties and have only been implemented in a limited number of oceanographic models to date [7, 8, 9, 10].

This paper presents details of an adaptive mesh, multi-scale model capable of simulating hydrodynamics and solute transport in coastal waters. The nesting procedure and the implementation of the adaptive mesh scheme are described. The adaptive mesh model (AMM) was applied to a large bay on the west coast of Ireland (Galway Bay) and used to simulate coliform discharges from a wastewater treatment plant (WWTP). AMM performance was assessed by comparing results with those from a high resolution single grid model and a static grid nested model, as well as measured data. A brief overview of the adaptive mesh procedure is provided. The modelled scenario and model configurations are described in detail and a selection of model results is presented and discussed. The results show that the AMM was able to accurately predict coliform transport whilst giving significant cost savings over both the single grid model and the classical static grid nested model.

2 Model Details

The AMM is based on the DIVAST (depth integrated velocity and solute transport) model. It is a two-dimensional, depth-averaged, finite difference model with coupled hydrodynamic and solute transport modules.

2.1 Governing Equations

The hydrodynamics module computes water surface elevations and depth-integrated velocities by solving the depth-integrated continuity and momentum equations. The continuity and x-direction momentum equations are expressed by (1) and (2) respectively as follows:

$$\frac{\partial \zeta}{\partial t} + \frac{\partial q_x}{\partial x} + \frac{\partial q_y}{\partial y} = 0 \qquad (1)$$

$$\frac{\partial q_x}{\partial t} + \beta\left[\frac{\partial U q_x}{\partial x} + \frac{\partial V q_y}{\partial y}\right] = \tag{2}$$
$$fq_y - gH\frac{\partial \zeta}{\partial x} + \frac{\tau_{xw}}{\rho} + \frac{\tau_{xb}}{\rho} + 2\frac{\partial}{\partial x}\left[\varepsilon H\frac{\partial U}{\partial x}\right] + \frac{\partial}{\partial y}\left[\varepsilon H\left[\frac{\partial U}{\partial y} + \frac{\partial V}{\partial x}\right]\right]$$

where, ζ = water surface elevation above mean water level
t = time
q_x, q_y = depth-integrated velocity flux components in the x,y directions
β = momentum correction factor
U, V = depth-integrated velocity components in the x,y directions
f = Coriolis parameter
g = gravitational acceleration
H = total depth of water column
τ_{xw} = surface wind shear stress components in the x direction
τ_{xb} = bed shear stress component in the x direction
ρ = fluid density
ε = depth averaged turbulent eddy viscosity

Solute transport processes are incorporated into the model using the 2D, depth-integrated advective-diffusion equation:

$$\frac{\partial H\phi}{\partial t} + \left[\frac{\partial HU\phi}{\partial x} + \frac{\partial HV\phi}{\partial y}\right] - \frac{\partial}{\partial x}\left[HD_{xx}\frac{\partial \phi}{\partial x} + HD_{xy}\frac{\partial \phi}{\partial y}\right] \tag{3}$$
$$-\frac{\partial}{\partial y}\left[HD_{yx}\frac{\partial \phi}{\partial x} + HD_{yy}\frac{\partial \phi}{\partial y}\right] - H\left[S_o + S_d + S_k\right] = 0$$

where, ϕ = solute concentration
[D_{xx}, D_{xy}, D_{yx}, D_{yy}] = depth-integrated dispersion-diffusion coefficients in the horizontal planes
S_o = source or sink input
S_d = first order decay rate or growth rate of the solute
S_k = total kinetic transportation rate

A space-staggered orthogonal grid system is used with ζ and ϕ specified at the centre of the grid cell and q_x, U, H_x and q_y, V, H_y specified at the centres of the x- and y-direction cell faces respectively. The finite difference scheme used in the model is based upon the Alternating Direction Implicit (ADI) technique which involves the sub-division of each timestep into two half-timesteps. Values of ζ, q_x and ϕ are therefore computed for the first half-timestep and ζ, q_y and ϕ are computed for the second half-timestep.

2.2 Nesting

Multi-scale modelling for structured grids involves nesting higher resolution child grids (CG) in lower resolution parent grids (PG). The AMM uses an overlapping grid structure and allows multiple levels of nesting so that child grids may be telescoped to any depth (i.e. a parent grid may contain one or more child grids and each child grid, in turn, may successively contain one or more child grids). Figure 1 shows an example of the grid structure. The nested model effectively consists of a series of parent and child models, dynamically linked and running simultaneously, where each model operates on the set of grids at a particular level of nesting. The open boundary conditions for each child grid are obtained from its parent using an adaptive linear interpolation scheme and are assigned to the child grid using a Dirichlet boundary condition. For each pair of parent and child grids, the time level of the child grid must be the same as that of the parent grid before the parent grid can be integrated forward in time. The nesting procedure is one-way, that is, the parent grid can influence the child grid but the child grid cannot influence the parent.

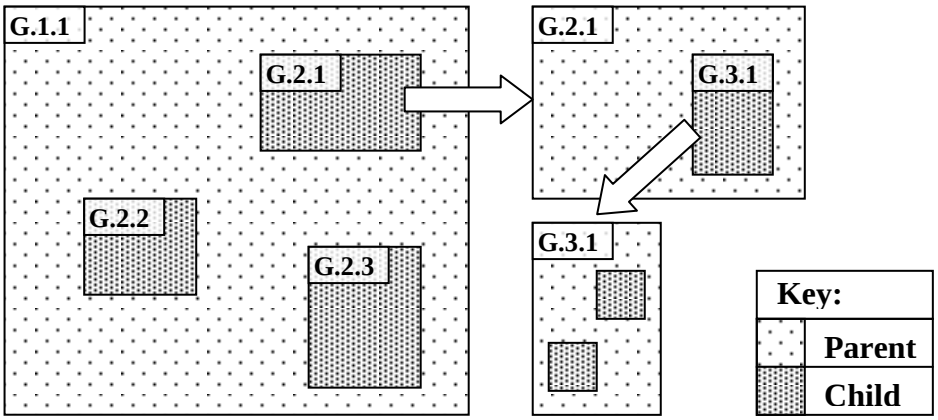

Figure 1: Nested model grid structure for multiple nesting.

The model allows any integer spatial nesting ratios; however, an odd nesting ratio such as the 3:1 ratio used in Figure 2 is preferable as it ensures that each grid value of the overlapping region of a parent grid coincides with a value from its child grid and simplifies the interpolation of boundary data. Although the model allows for different spatial and temporal nesting ratios, the same ratio is typically used for both. Linear interpolation is used for time-wise interpolation. The CG boundary interface is two CG cells in width; the inner layer of grids cells are the internal boundary cells and the outer layer are the ghost cells. This boundary configuration has been shown to have excellent conservation properties [11]. Only the components of velocity and flux normal to the boundary must be specified at ghost cells whilst all prognostic variables must be specified at internal boundary cells.

2.3 Adaptive Meshing

The AMM was developed so that any child grid can be either static or adaptive. The movement of an adaptive CG may be predetermined by the user (specified) or automatically controlled by the model (automatic). The size and shape of the adaptive CG can be altered upon movement so that the required area of high resolution can be minimised. In addition, a new CG can be generated at any time during the simulation. For specified movement, the timing of each move and the new grid location after a move are defined by the user in the input data file; for automatic movement, the timing and extent of each move is controlled by a predetermined tracking algorithm.

At the end of each PG timestep all adaptive child grids must be checked to see if adaption is required. Following adaption, a CG must be re-initialised. A common data region exists where the old and new grid configurations overlap (Figure 2). Data from grid cells within this region for the old configuration are transplanted to the appropriate locations in the new grid configuration. A second region also exists in the new grid which has no data. Data for this region are obtained by interpolation of PG data; an inverse distance weighted interpolation scheme is used for this process. It is important to monitor adaptive CG movements during the course of a simulation. A CG cannot be permitted to move outside its parent's boundaries as it would then have multiple parents supplying multiple sets of boundary data. Neither can one CG be allowed to overlap another CG at the same level of nesting. If either situation were to occur as a result of a potential move, the move is prohibited.

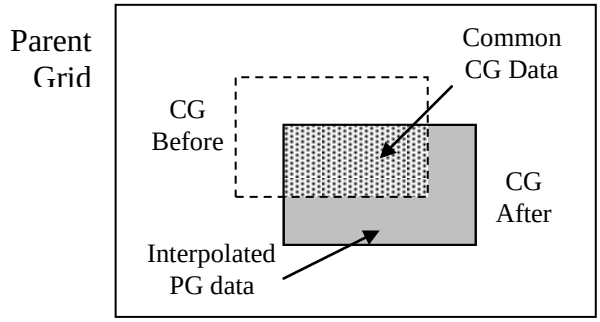

Figure 2: CG configurations before (dashed) and after (solid) adaption. Dotted area is region of common data and shaded area is region of interpolated PG data.

3 Model Application

Galway Bay was the test case for the AMM. The bay, shown in Figure 3, is a large macro-tidal bay on the west coast of Ireland. The inner bay is relatively shallow with depths less than 30m below spring high water (SHW). The outer bay extends seaward to the Aran Islands and gradually deepens to approximately 60m in the passages to the northwest and southeast of the islands where it meets the Atlantic Ocean. The typical ranges of spring and neap tides are 5m and 2m respectively.

AMM performance was assessed by comparing results with those from a single grid high resolution model of the bay. The single grid model of the bay (SG_100), considered the 'correct' model solution, covered the extents of the domain shown in Figure 3 at 100m spatial resolution. The domain size was approximately 57x33 km^2 and contained almost 190,000 grid cells. The AMM consisted of a parent grid (PG) with the same grid extents as SG_100 and a single child grid (CG) at a 3:1 nesting ratio. The PG was resolved at 300m and the child grid was resolved at 100m to correspond to the resolution of SG_100. The model parameters are summarised in Table 1.

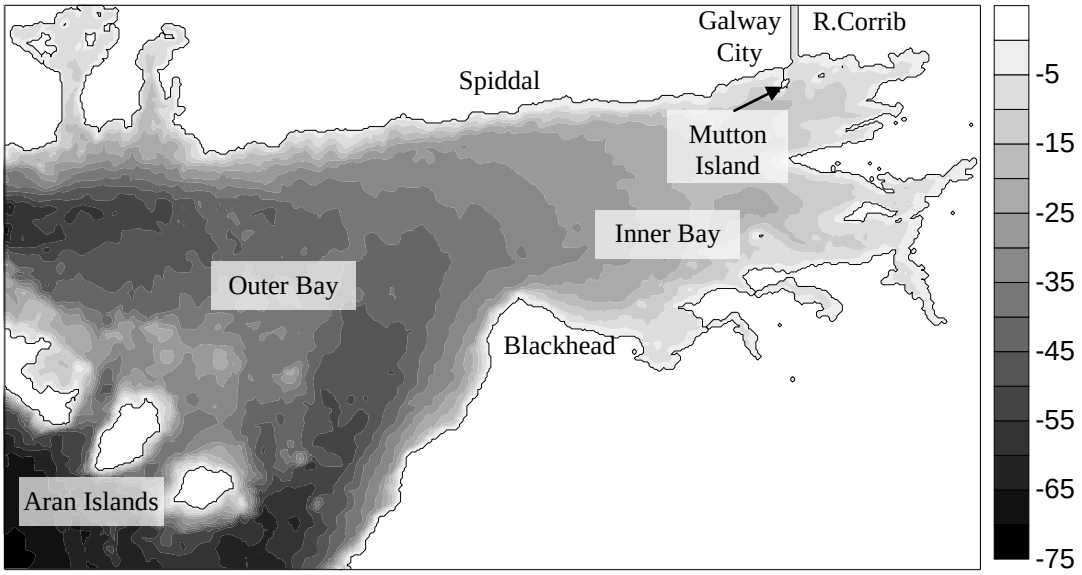

Figure 3: Plan view of Galway Bay model domain (depths in m below SHW).

Physical Parameter	**SG_100**	**AMM**	
		PG	**CG**
L_X	57 km	57 km	variable
L_Y	33.3 km	33.3 km	variable
Tidal Amplitude:			
- spring	2.5 m	2.5 m	2.5 m
- neap	1.0 m	1.0 m	1.0 m
Tidal Period	12.5 hrs	12.5 hrs	12.5 hrs
Resolution:			
- grid spacing	100 m	300 m	100 m
- timestep	20 s	60 s	20 s
No. of grid cells	189,810	21,090	variable
Bed Roughness	200 mm	200 mm	200 mm

Table 1: Summary of Galway Bay models.

3.1 Scenario Details and Input Data

The AMM was used to model the transport and fate of faecal colifirms resulting from WWTP discharge into Galway Bay. Domestic and industrial sewage from Galway city is treated at Mutton Island WWTP. The treated effluent is discharged into the sea approximately 400m south of Mutton Island (see Figure 3) via an outfall pipe. Both input data and measured water quality data were available from a previous modelling study [12]. A time-varying modified first order decay rate model, first proposed by Mancini [13] and later modified by Harris [14], was employed for the faecal coliform decay rate, *k*. The formulation takes account of light, temperature, salinity, settling and acidity and may be expressed as:

$$k = F_P \frac{v_s}{H} + \left[\left[0.8 + 0.006(\%seawater) \right] x 1.07^{t_w - 20} + \frac{\alpha I_0}{K_e H} \left[1 - e^{-K_e H} \right] \right] \left[k_{pH}\, pH \right] \qquad (4)$$

where, F_P = fraction of attached bacteria
v_s = settling velocity (m/s)
t_w = water temperature (ºC)
α = constant of proportionality
I_o = irradiance at surface (W/m^2)
K_e = vertical light extinction coefficient (m^{-1})
k_{pH} = die-off rate due to pH (d^{-1})
pH = acidity

The die-off rate due to pH, k_{pH}, is further calculated as:

$$k_{pH} \approx 0.135 \cosh(0.445(6.5 - pH)) \qquad (5)$$

Table 2 lists the values used for the various parameters in equations (4) and (5). F_P and v_s were unknown for Galway Bay and were instead estimated from literature. The constant of proportionality α is a calibration parameter; its value of 0.32 was determined by Harrold [12] during model calibration. The surface irradiance was set to zero in the time between sunset and sunrise.

Parameter	Value
Fraction of attached bacteria, F_P	0.9
Settling velocity, v_s	1.2 m/d
Water temperature, t_w	17ºC
Constant of proportionality, α	0.32
Irradiance at surface, I_o	400 W/m^2
Light extinction coefficient, K_e	1.0 m^{-1}
pH	8.1

Table 2: Parameters used to calculate faecal coliform decay rate.

Hourly discharge rates from Mutton Is. WWTP were provided by Galway City Council for the period 02/08/08 – 06/08/08. The concentration of faecal coliforms in the effluent was not known. An estimated concentration of 50,000cnts was calculated based on a series of effluent water quality samples taken in 2007. Heavy rain was recorded in the region of Galway Bay on the morning of 05/08/08 from 9:00 – 10:00am with resulting storm flow discharge from the WWTP. The levels of faecal coliforms discharged during this period of time would have been much greater than normal; the event was incorporated in the modelled scenario by increasing the discharge concentration from 50,000cnts to 300,000cnts for the period of storm flow discharge. The appropriate tidal data was specified at the open sea boundaries of the model domain. A flow rate of $50m^3/s$ was specified at the River Corrib freshwater boundary; this was the monthly-averaged flow rate for August.

3.2 Model Simulations

Two AMM simulations were carried out. The first simulation employed a static child grid (CG_Static) and the results were used to determine baseline CG accuracy relative to the reference solution SG_100. The second simulation employed an adaptive child grid (CG_Adapt) and accuracy was analysed relative to both SG_100 and baseline CG accuracy. All coliform simulations were run for the same discharge scenario.

The boundaries of CG_Static were chosen so that the discharge plume was fully contained within the child grid for the duration of the simulation. The required grid extents were determined from PG plume results. To reduce CG errors CG_Static boundaries were placed in areas of high PG accuracy. Grid S in Figure 4 marks the extents of CG_Static. For CG_ Adapt, grid adaptions were specified at the beginning of the simulation in the form of move times and corresponding grid locations. These data were also determined from PG results by noting plume movements and extents during the course of the simulation. Selection of CG_Adapt extents was based solely on PG plume movements; PG accuracy at the proposed CG boundaries was not considered. Four timed moves were specified. Locations and extents of CG_Adapt at time zero and after each timed move are shown in Figure 4. The grid numbers in the diagram correspond to the following move times:

- Grid 1: 0 hrs
- Grid 2: 18.75 hrs
- Grid 3: 31.25 hrs
- Grid 4: 43.75 hrs
- Grid 5: 56.25 hrs
- Grid 5: 68.75 hrs

For model validation, water quality sampling data was available for 05/08/08. Samples were taken at five different locations at early-morning, midday and mid-afternoon; three samples were collected at each time giving 45 samples in total. Sampling locations (see Figure 5) were chosen to give a good cross-section of the effluent plume. Site 2 corresponded to the discharge location.

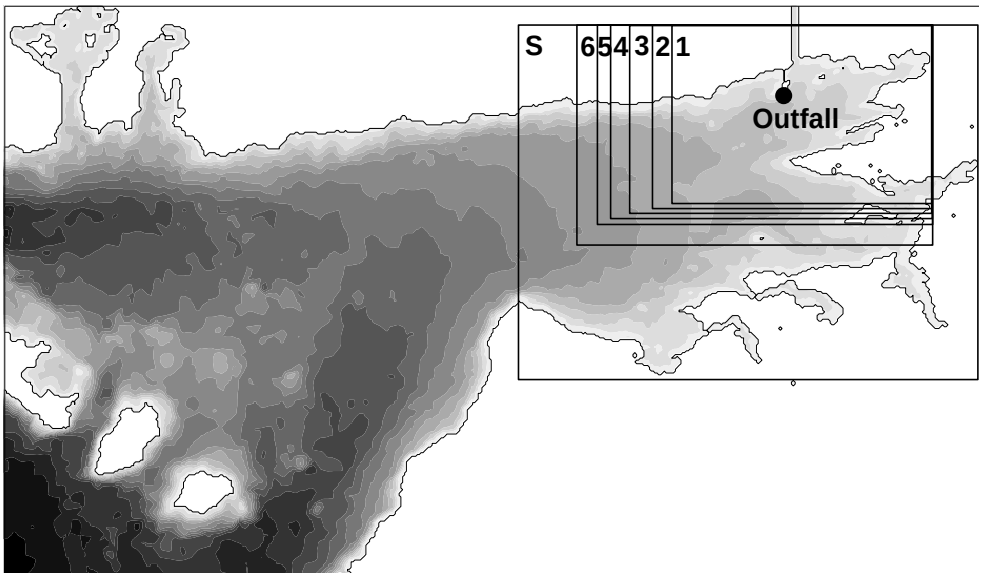

Figure 4: Grid configurations used in the AMM simulations; grid S was used for CG_Static, grids 1-6 were used for CG_Adapt.

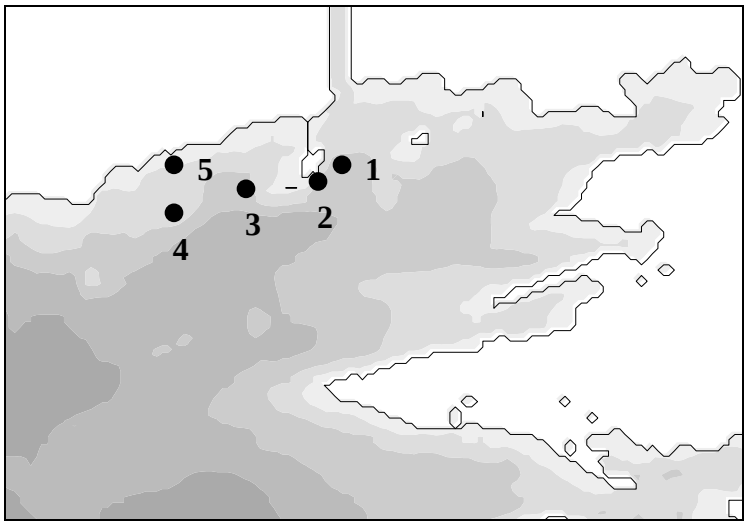

Figure 5: Water quality sampling sites; site 2 was at the discharge location.

4 Model Results

AMM accuracy was determined, firstly, relative to the SG_100 reference solution and, secondly, relative to the measured water quality data. AMM results were also compared to PG results to assess the improvement in accuracy resulting from the higher resolution of the nested grids in AMM.

4.1 Hydrodynamics

The results of the CG_Static simulation were used to determine the accuracy of AMM hydrodynamics. CG_Static velocities were compared to both PG and SG_100 velocities. Figure 6 compares current velocity timeseries at Site 2 and Site 4; linear regression analyses of the datasets are also shown. It can be seen that AMM velocities showed excellent correlation with SG_100 velocities; r^2 values of 1 were calculated at both sites. The slopes and y-intercepts of the CG_Static trendlines provided further evidence of CG accuracy. The improvement in accuracy from PG to CG was readily apparent from both the timeseries comparisons and the regression analyses; r^2 values of just 0.76 and 0.89 were calculated for PG velocities at Site 2 and Site 4 respectively. Similar levels of CG_Static accuracy at Sites 1, 3 and 5.

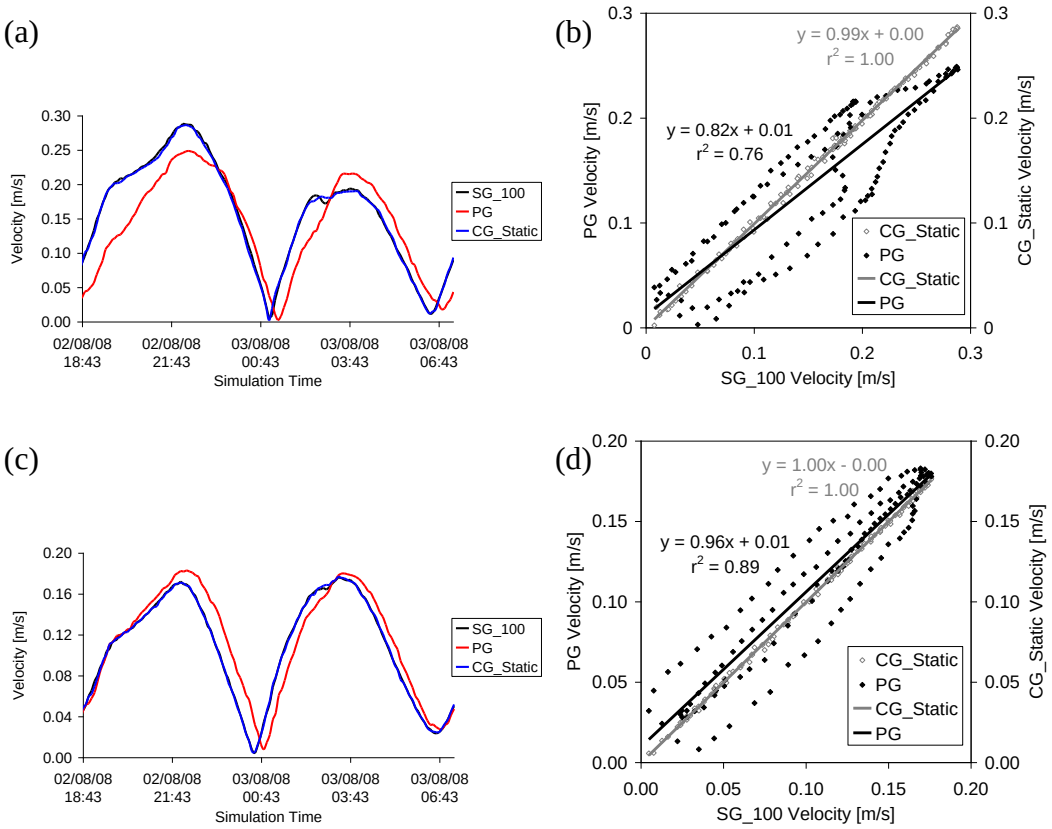

Figure 6: Velocity comparisons and LR analyses at (a, b) Site 2 and (c, d) Site 4.

4.2 Mass Transport

Four different sets of coliform results were available for comparison from the model simulations: SG_100, PG, CG_Static and CG_Adapt. Model results consisted of snapshots of plume extents and timeseries of coliform counts at the sampling sites. The measured data was available for the period during and after the storm flow

discharge which took place on the morning of 05/08/08. Snapshots were output from the model at hourly intervals for a period of 24 hours after the hour-long discharge ended (10:00hrs). Timeseries data were output over the full simulation period. Due to space limitations, only a small selection of results can be presented.

Figure 7 compares snapshots of plume extents +19hrs after storm flow discharge for the four model simulations. A clear difference in SG_100 and PG model results is visible. PG plume shape and extents and concentration gradients were all quite different than those of SG_100. The differences in mass transport were a result of the less accurate PG hydrodynamics which, in turn, were a direct consequence of the lower PG resolution. In contrast, both the CG_Static and CG_Adapt simulations produced solute plumes that compared well with SG_100 plumes. CG plume shape and extents, and coliform gradients and concentrations were almost identical to those of SG_100. Comparison of coliform plumes at other output times confirmed the lower accuracy of PG results and the higher accuracy of CG results. In addition to the improved accuracy of CG results, the results of CG_Adapt were also quite similar to those of CG_Static, indicating that any errors introduced as a result of the adaptive meshing were quite low.

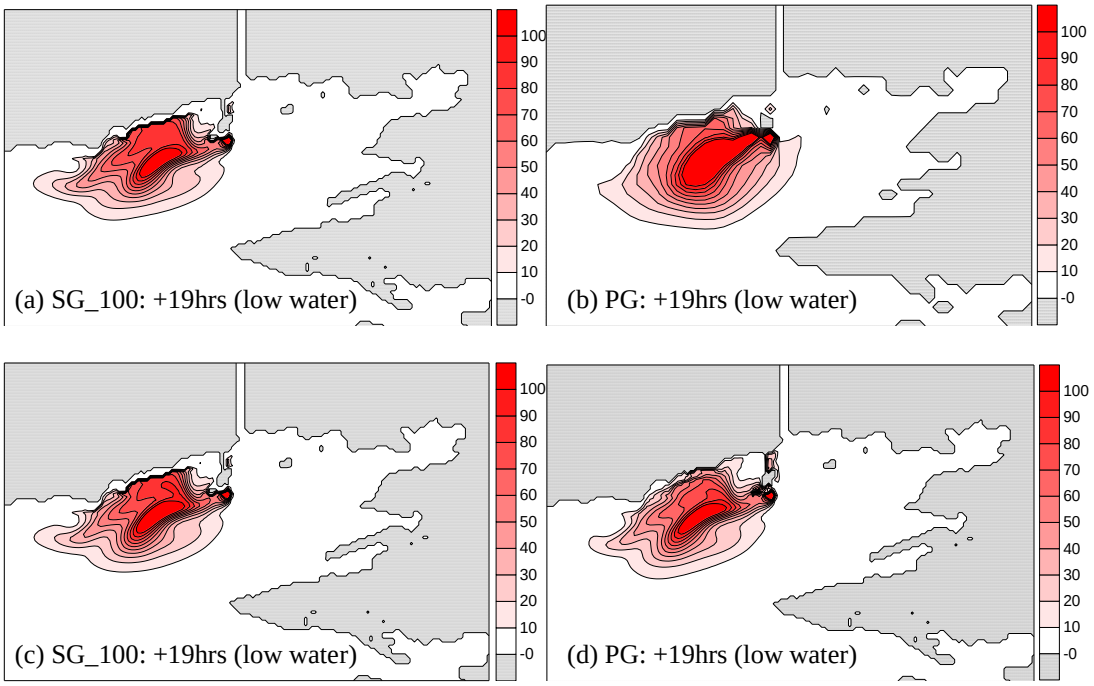

Figure 7: Comparison of coliform plumes +19hrs after storm flow discharge.

To further assess the accuracy of PG and CG results, timeseries of coliform counts were compared at the five sampling sites. Figure 8 shows the timeseries comparisons at site 2, the point of discharge, for a 24-hour period spanning the time before, during and after the storm flow discharge. The inaccuracy of PG is clearly visible. From Figure 8a it can be seen that SG_100 was highly accurate and showed

excellent correlation with the measured data. Relative to SG_100, PG demonstrated high levels of error for a large proportion of the simulation time. The peak concentration recorded during storm flow discharge by SG_100 was 2,338cnts compared to 1,930 by PG; an absolute error of 408cnts or a relative error of 17%.

In contrast, it can be seen from Figure 8b that the coliform timeseries from both CG solutions compared well with SG_100 for the full 24-hr period shown. While differences in peak concentration during the storm flow discharge were observed, they were quite low. Peak concentration in CG_Static was 2,466cnts giving an absolute error of 128cnts or relative error of 5%; peak concentration in CG_Adapt was 2,502cnts giving an absolute error of 164cnts or a relative error of 7%. Correlation of CG coliform counts with the measured data was also good. Similar levels of CG accuracy were observed at the other four sampling sites.

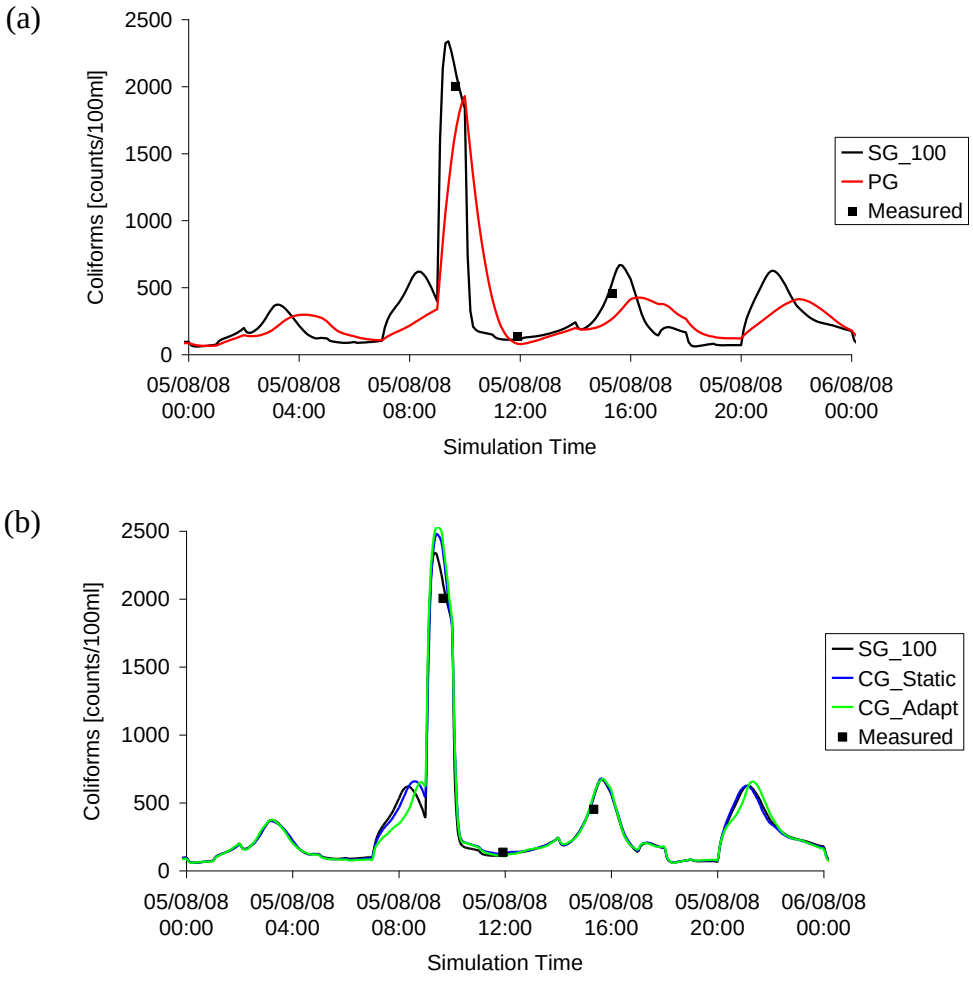

Figure 8: Comparison of coliform concentration timeseries at Site 2.

AMM results were extremely positive. They proved that the adaptive mesh capability of the AMM functioned correctly and that the model achieved similar

levels of accuracy to the reference model. The results confirmed that the AMM was capable of simulating flow regimes and resulting mass transport to a high degree of accuracy in a highly resolved area of interest. In relation to computational savings, the AMM achieved significant efficiencies compared to the high resolution single grid model of Galway Bay. An 84% reduction in computational cost was recorded for CG_Adapt relative to SG_100 (71 mins compared to 457 mins). Most importantly, this represented an additional 10% computational savings compared to the savings achieved by the classical static grid nesting approach.

5 Summary and Conclusions

An adaptive mesh, multi-scale model for tidal hydraulics and mass transport in coastal waters was developed and tested. Model performance and accuracy was assessed by simulating coliform discharges from a WWTP in Galway Bay. Two different nested grid configurations were used to assess the performance and accuracy of the AMM. The first was a single static child grid, CG_Static. This configuration was used to obtain base-line CG accuracy. The second configuration was an adaptive child grid, CG_Adapt. The adaptions of CG_Adapt were user-specified with CG move-times and extents determined from plume movements computed by the lower resolution PG model.

The results of CG_Adapt were compared with those from CG_Static and the high resolution SG_100. Both child grid solutions were found to be superior to the lower resolution PG solution and both showed excellent correlation with the SG_100 reference solution and measured data. High levels of CG accuracy were observed for both hydrodynamics and coliform transport. CG boundary locations for the adaptive meshes were selected based solely on the plume behaviour of the PG model; PG accuracy was not taken into account. While this meant that PG errors could be introduced to the CG_Adapt solution via the boundary data, they did not adversely affect model accuracy in the AOI and the accuracy of CG_Adapt was similar to that of CG_Static.

It can be concluded that adaptive mesh nesting approaches can offer additional computational efficiencies over classical static grid nesting approaches; an additional 10% reduction in computational cost was recorded in the case of the AMM. However, careful planning is required for the application of adaptive meshes. It is recommended that moves are user-specified, as opposed to automated, and that the moves are planned using correct CG boundary placement procedures based on PG accuracy, otherwise significant degradation of model accuracy might occur. For optimum model performance, changes in grid extents for adaptive meshes should be informed by analysis of hydrodynamic and water quality results from the lower resolution PG model.

References

[1] A.D. Fox and S.J. Maskell, "Two-way interactive nesting of primitive equation ocean models with topography", Journal of Physical Oceanography 25: 2977-2996, 1995.
[2] J. Pullen and J.S. Allen, "Modeling studies of the coastal circulation off the northern coast of California: statistics and patterns of wintertime flow", Journal of Geophysical Research 106(C11): 26,959-26,984, 2001.
[3] J. Staneva, E.V. Stanev, J.O Wolff, T.H. Badewien, R. Reuter, B. Flemming, A. Bartholoma and K. Boldinge, "Hydroynamics and sediment dynamics in the German Bight. A focus on observations and numerical modelling in the East Frisian Wadden Sea", Continental Shelf Research 29: 302-319, 2009.
[4] G.W. Ley, and R.L. Elsberry, "Forecasts of Typhoon Irma using a nested-grid model", Monthly Weather Review 104: 1,154–1,161, 1976.
[5] Y. Kurihara, G.J. Tripoli, and M.A. Bender, "Design of a movable nested-mesh primitive equation model", Monthly Weather Review 107: 239–249, 1979.
[6] M.A. Bender, I. Ginis, R. Tuleya, B. Thomas and T. Marchok, "The operational GFDL coupled hurricane-ocean prediction system and summary of its performance", Monthly Weather Review 135(12): 3,965-3,989, 2007.
[7] E. Blayo and L. Debreu, "Adaptive mesh refinement for finite-difference ocean models: first experiments", Journal of Physical Oceanography 29: 1239-1250, 1999.
[8] C. Rowley and I. Ginis, "Implementation of a mesh movement scheme in a multiply nested ocean model and its application to air–sea interaction studies", Monthly Weather Review 127: 1,879-1,896, 1999.
[9] A.G.L. Borthwick, S. Cruz León and J. Józsa J, "The shallow flow equations solved on adaptive quadtree grids", International Journal for Numerical Methods in Fluids 37(6): 691–719, 2001.
[10] A. Herrnstein, M. Wickett and G. Rodrigue, "Structured adaptive mesh refinement using leapfrog time integration on a staggered grid for ocean models", Ocean Modelling 9: 283–304, 2005.
[11] S. Nash and M. Hartnett, "Nested circulation modelling of inter-tidal zones: details of a nesting approach incorporating moving boundaries", Ocean Dynamics 60: 1,479-1,495, 2010.
[12] B. Harrold, "Bacteriological modelling of Galway Bay", M.Eng.Sc. Dissertation, Civil Engineering, College of Engineering and Informatics, National University of Ireland Galway, 2010.
[13] J.L. Mancini, "Numerical estimates of coliform mortality rates under various conditions", Water Pollution Control Federation 50(11): 2,477–2,484, 1978.
[14] E.L. Harris, "Environmental hydro-informatics tools for water quality management", Ph.D. Dissertation, Division of Civil Engineering, Cardiff School of Engineering, University of Cardiff, 2003.